Nanoscale

Accepted Manuscript

This article can be cited before page numbers have been issued, to do this please use: J. Gao, M. Chen, W. Wen, X. Zhang, S. Wang and W. Huang, *Nanoscale*, 2019, DOI: 10.1039/C9NR02190F.

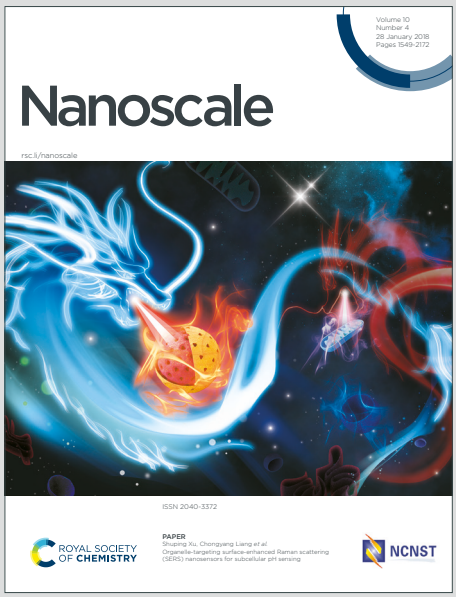

ROYAL SOCIETY OF CHEMISTRY

rsc.li/nanoscale

View Article Online
DOI: 10.1039/C9NR02190F

Nanoscale

ARTICLE

Au-Luminol Decorated Porous Carbon Nanospheres for Electrochemiluminescence Biosensing of MUC1

Received 00th January 20xx,
Accepted 00th January 20xx

DOI: 10.1039/x0xx00000x

www.rsc.org/

Jing-Wen Gao,[a] Miao-Miao Chen,*[a,b] Wei Wen, [a] Xiuhua Zhang,[a] Shengfu Wang,[a] and Wei-Hua Huang[b]

Electrochemiluminesence (ECL) nanomaterials are usually deposited compactly on the surface of electrodes, which may cause poor mass transfer of reactants and results in low ECL efficiency. In this work, we developed a novel kind of luminescent materials denoted as C-Au-luminol nanospheres (C-Au-Lum NSs) by highly dispersion of luminophores on porous carbon nanospheres (PCNSs). C-Au-Lum NSs were facilely prepared by in situ reduction of chloroauric acid with luminescent reagent luminol (Lum) on the nano-pores of PCNS. Plenty of luminescent Au-Lum NPs are dispersedly concentrated inside the numerous pores and hollow interiors of PCNSs, effectively increasing mass transfer of regents and accelerates electron transport inside porous nanospheres. This greatly improves availability of luminophores and endowing the C-Au-Lum NSs with excellent ECL emission. Further integrating with of enzymatic circulation and strand displacement, an ultrasensitive ECL biosensor was achieved for ultrasensitive detection of an important tumor biomarker, mucin1. A logarithmically linear range from 0.1 pg/mL to 1 ng/mL with the detection limit of 47.6 fg/mL (S/N = 3) were achieved, demonstrating the superior performance of the C-Au-Lum NSs. This work would provide new ideas in construction of high-performance ECL sensing platforms for diverse applications.

Introduction

Mucin1 (MUC1) is a transmembrane glycoprotein over-expressed in most malignant tumors originated from different cancerous organ such as breast, lung, pancreas or stomach. The abnormal expression of MUC1 protein could happen at the entire cancer cell surface, and also exist in cancer patients' blood as MUC1 fragments.[1-4] The extremely low level of MUC1 has been acted as a potential biomarker at very early stage of tumors. Hence, it is urgently needed to develop highly sensitive and selective method to detect MUC1 for early diagnosis and prognosis assessment in adenocarcinomas. Nowadays various techniques including surface-enhanced raman scattering[5], enzyme linked immunosorbent assay[6], fluorescence[7], photoelectrochemical[8], electrochemical method[9] and electrochemiluminescence (ECL)[10, 11] have been established to quantify trace amounts of MUC1. Thereinto, ECL as an electro-generated chemiluminescence process has captured increasing attention due to its accurate controllability, free light source and high sensitivity.[12-17] For instance, ECL resonance energy transfer system from Ru(II) complex to graphene oxide[10], and mesoporous luminescence-functionalized metal-organic frameworks[11] have been successfully used to sensitively detect MUC1 protein.

For a given ECL system, ECL intensity strongly relies on the quantity and availability of luminophores on the electrode surface.[15,17,18] Great achievements have been made to prepare highly efficient luminescent nano-materials by loading multifarious luminophores (e.g. ruthenium (II) complexes[17, 19, 20], quantum dots[18, 21], luminol[22, 23]) onto the surface or inner of nano-materials. Immobilization of such luminescent nano-materials effectively improves both the quantity and availability of luminophores, and therefore enhances the ECL intensity as compared with ECL systems where luminophores are dispersed in solutions. However, the luminescent nano-materials are usually compactly deposited on the electrode surface, which consequently cause poor mass transfer inside the nano-assembly and restricts availability of the luminophores. In this regard, development of loading strategies capable of highly dispersed immobilization of large amounts of luminescent nano-materials is of vital importance. When luminophores are densely immobilized but strictly decentralized on the sensing interface, the mass transfer rate could be rapidly accelerated and the ECL emission is hereafter enhanced.[24, 25] Moreover, the conductivity of the loading materials is also a critical issue, and materials with the superior conductivity would greatly facilitate the electron transfer and further boost the ECL signal.

[a] Hubei Collaborative Innovation Center for Advanced Organic Chemical Materials, Ministry of Education Key Laboratory for the Synthesis and Application of Organic Functional Molecules & College of Chemistry and Chemical Engineering, Hubei University, Wuhan 430062, China. E-mail: chen_mm@whu.edu.cn
[b] Laboratory of Analytical Chemistry for Biology and Medicine (Ministry of Education), College of Chemistry and Molecular Sciences, Wuhan University, Wuhan 430072, China.
Electronic Supplementary Information (ESI) available. See DOI: 10.1039/x0xx00000x

View Article Online
DOI: 10.1039/C9NR04105F

Porous materials, such as metal–organic frameworks[26, 27], cellulose paper[28] and carbon[29, 30], possess many satisfactory merits such as well-defined porous structure, large surface area, and tailor-made pores with functions[31]. With these superiorities, porous materials have received increasing application in numerous fields including medicine delivery[32], sensors[33], heterogeneous catalysis[34], and energy storage[35]. The abundant pore construction could afford sufficient probe materials efficaciously and reinforce the diffusion of reactants.[34, 36-39] This greatly improved the overall sensing materials availability and lowered internal mass transfer limitations, resulting in ECL signal enhancement.[40-42] Among various porous materials, porous carbon nanospheres (PCNSs) not only provide porous carriers for highly disperse immobilization of probe materials, but also have excellent conductivity and stability[29, 43, 44]. In this regard, PCNSs can be served as promising carrier materials to construct highly sensitive ECL sensing system.[42]

In this study, a kind of PCNSs with well-defined and hollow structure was synthesized and used as the carrier for loading luminophores to construct an ultrasensitive ECL sensing platform. The composite nanospheres (denoted as C-Au-Lum NSs) were prepared by in situ reduction of chloroauric acid with luminescent reagent luminol (Lum) to form gold-Lum nano-particles (Au-Lum NPs) on the nano-pores of PCNSs carrier (Figure 1A). Through this design, plenty of luminescent materials Au-Lum are dispersedly concentrated inside the numerous pores and hollow interiors of PCNSs. This effectively increases mass transfer and accelerates electron transport inside porous nanospheres, therefore greatly improving availability of luminophores and endowing the C-Au-Lum NSs with excellent ECL emission performance. Further integrating with proximity-initiated secondary target DNA strand displacement (Figure 1B) and endonuclease-assisted recycling amplification strategy (Figure 1C), an ultrasensitive ECL biosensor has been developed for detection of MUC1. This work discloses a novel luminescent nanocomposite by incorporating porous carbon materials, and may provide new ideas in construction high-performance ECL sensing platforms for diverse applications.

Experimental

Reagents and Apparatus.

MUC1 was purchased from Shanghai Jianglai Industrial Limited By Share Ltd (China). Luminol, Gold (III) chloride trihydrate

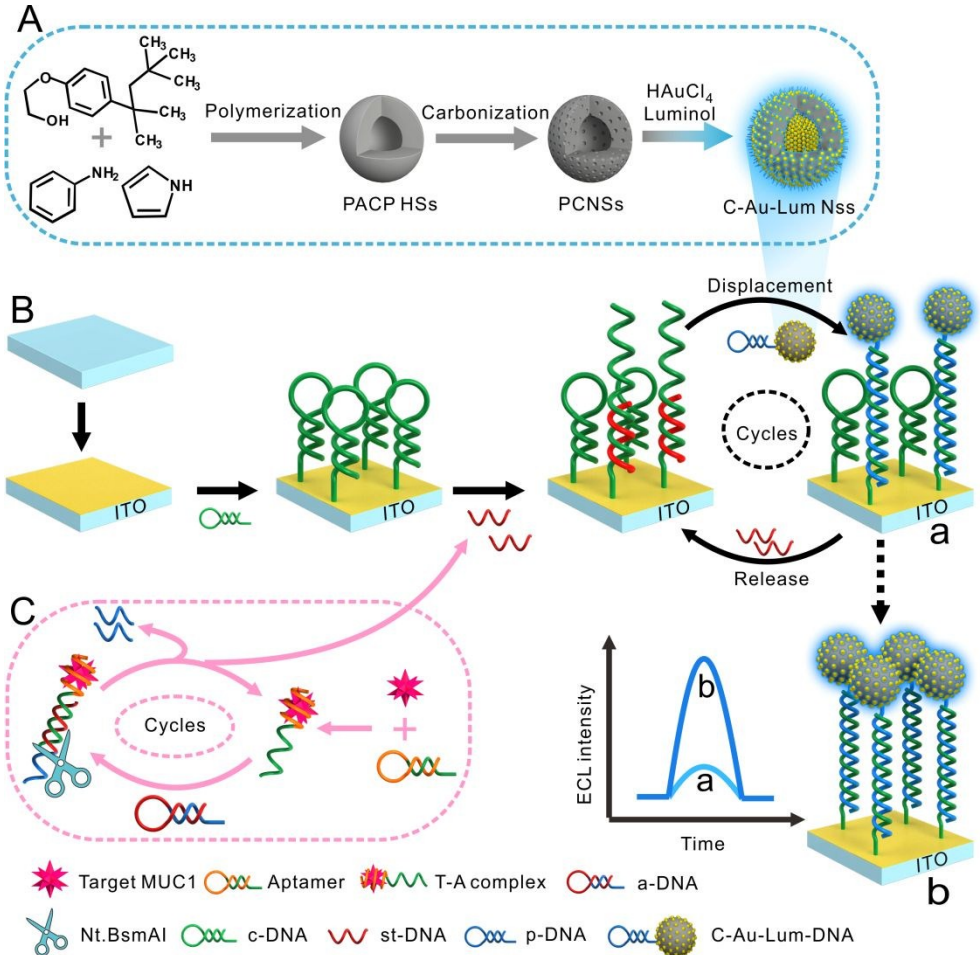

Figure 1. Schematic Illustration of ECL biosensors for MUC1 detection: (A) Design and Fabrication of novel C-Au-Lum NSs Nanomaterials, (B) Fabrication of the Biosensor and the Strain Displacement Circulation for MUC1 Target Detection; (C) MUC1 recognition and Nt.BsmAI-Assisted Recycling Amplification Process.

($HAuCl_4 \cdot 3H_2O$) and thrombin (Tb) were obtained from Sigma-Aldrich (Beijing, China). Tris (2-carboxyethyl) phosphine hydrochloride (TCEP), sodium hydroxide (NaOH), trisodium citrate, hydrogen peroxide solution (H_2O_2, 30 wt%), bovine serum albumin (BSA), aniline, pyrrole, triton X-100, ammonium persulfate ($(NH_4)_2S_2O_8$) and 6-mercapto-1-hexanol (MCH) were purchased from Aladdin Industrial Company (Shanghai, China). Nt.BsmAI was bought from New England Biolabs (Ipswich, USA). Myoglobin (Mb) and carcinoembryonic antigen (CEA) were purchased from Abcam (England). Ethanol was obtained from Sinopharm Chemical Reagent Co. (Shanghai, China). All other reagents were of analytical reagent grade and used without further purification. The ultrapure water (18.25 MΩ•cm) was used during the whole experiment. The human serum was obtained from Zi-Jing hospitial (Wuhan city, Hubei province). All the experiments were implemented according to the relevant laws and institutional guidelines of China and were approved by the ethics committee at Hubei University. Informed consent was obtained from the human participants of this study.

The synthetic single-stranded oligonucleotides were purchased from Shanghai Sangon Biotechnology Co. (Shanghai, China) and the sequences of oligonucleotides were as follows and also shown in Table S1:

Aptamer (for MUC1): 5'-GCAGTTGATCCTTTGGATACCCTGGCG -ATCAACTGCGAGAGACTT-3'

Auxiliary-DNA (a-DNA): 5'-AAGTCTCTCGCAGTTTAGAC-3'

Capture DNA (c-DNA): 5'-SH-GTCTAAACTGCGGCCACAGAACTG -CAGT-3'

Probe-DNA (p-DNA): 5'-SH-AAAACTGCAGTTCTGTGGCCGCAGTT -TAGAC-3'

The DNA hairpin structure involved in this study was formed by heating to 95 °C for 5 min and then cooling to room temperature naturally.

ECL-potential or ECL-wavelength profile was measured on a model MPI-A ECL analyzer (Xi'An Remax Electronic Science &Technology Co. Ltd., Xi'An, China) with AOL-1 full spectrum detector. High resolution transmission electron microscope (HRTEM, JEM-2100, Japan) and scanning electron microscopy (SEM, Zeiss Sigma field-emission, Germany) were recorded for characterization of morphologies. X-ray photoelectron spectroscopy (XPS) measurements were conducted with a Thermo Scientific, ESCALAB 250Xi. Ultraviolet-visible spectrophotometer (UV-2700, Shimadzu, Japan) and Fluorescent spectrophotometer (RF-5301PCShimadzu, Japan) were used. Electrochemical experiments including electrodeposition and electrochemical impedance spectroscopy (EIS) were performed on a CHI 660E electrochemical workstation (Shanghai Chenhua Instruments Inc., China).

Synthesis of PCNSs and C-Au-Lum NSs

PCNSs were synthesized by direct carbonization of hollow polymer spheres (HPSs) according to previous literature reports with simple modifications.[29] Simply, 3.80 mL of aniline and 2.90 mL of pyrrole were added to vigorously stirred 600 mL of deionized water containing 0.60 g of Triton X-100, forming a homogeneous pale-yellow micelle solution. Next, the precooled $(NH_4)_2S_2O_8$ solution as an initiator was added dropwise to the above solution for 12 h at 6 °C. Followed by vacuum filtration and washed with ultrapure water, HPSs were obtained. After dried at 80 °C for 12 h, the HPSs were heated (900 °C, 10 h) in a furnace at the ramp rate of 5 °C/min under a N_2 flow. After carbonization, the gained black powder was PCNSs used for further experiments.

C-Au-Lum NSs was prepared for the first time based on the previous reported synthesis method of Au-Lum[45]. In details, 100 μL of 10.0 wt% $HAuCl_4$ solution was mixed with 100 mL of PCNSs suspension in freshly prepared clean round bottom flask under stirring, and then treated by sonication for 30 min at room temperature. Subsequently, when the above mixture was heated to boiling, 1.60 mL of 0.01 M luminol solution was added rapidly under vigorous stirring. The solution was maintained at the boiling status for 30 min. The obtained colloid was kept at room temperature under slightly stirring for 1 h. The resultant products were centrifuged (12000 rpm, 10 min) and purified with ultrapure water in succession for 2 times to remove the unbounded luminol or Au-Lum NPs, and then stored at 4 °C for the further use. Moreover, 1.60 mL of 0.01 M luminol or 2.70 mL of 1 wt% trisodium citrate was severally added to the boiled 0.01 wt% $HAuCl_4$ solution without PCNSs to obtain Au-Lum NPs or Au NPs under the same other conditions.

Fabrication of the proposed biosensor

C-Au-Lum-DNA conjugates were prepared as follows: a certain volume of thiolated hairpin probe (10 μM) was added into 1 mL C-Au-Lum NSs suspension containing 0.2 mM TCEP and stirred for 5 h at room temperature. Afterwards, 100 μL of 10 wt% BSA solution was introduced into the mixture to block the unoccupied sites of C-Au-Lum NSs. Subsequently, the obtained C-Au-Lum-DNA conjugates were centrifuged for 10 min with 11000 rpm and washed with Tris-HCL buffer solution (10mM, pH 7.4). The precipitates were suspended with 250 μL of Tris−HCl buffer and then stored at 4 °C.

The secondary target DNA was prepared by the following steps. First, 100 μL different concentrations of target MUC1 was incubated with 100 μL aptamer (2 μM) at 37 °C for 1 h. The obtained product was named as T-A complex. Then, 20 μL a-DNA (10 μM) and a certain concentration of Nt.BsmAI endonuclease were added into the above mixture. The solution was incubated at 37 °C for a period of time. The a-DNA (5'-AAGTCTCT ▼ CGCAGTTTAGAC-3') and T-A complex could form partly complementary DNA complex containing specific site[46]. Meanwhile numerous secondary target DNA (st-DNA) fragments were released and the enzyme-assisted T-A complex recycling process was completed. Thereafter, Nt.BsmAI was inactivated by heating the system to 65 °C for 20 min and cooled to room temperature naturally. Hence, a large number of intermediate DNA was obtained.

Prior to modification, the ITO electrode was cleaned thoroughly by sonicating in anhydrous ethanol and ultrapure water, respectively. After the cleaned electrode was dried naturally, it was immersed into 1 wt% $HAuCl_4$ and

electrodeposited at -0.2 V for 60 s. After that, the electrode was incubated with 25 μL of 1 μM c-DNA containing 0.2 mM TCEP at room temperature overnight, followed by incubating

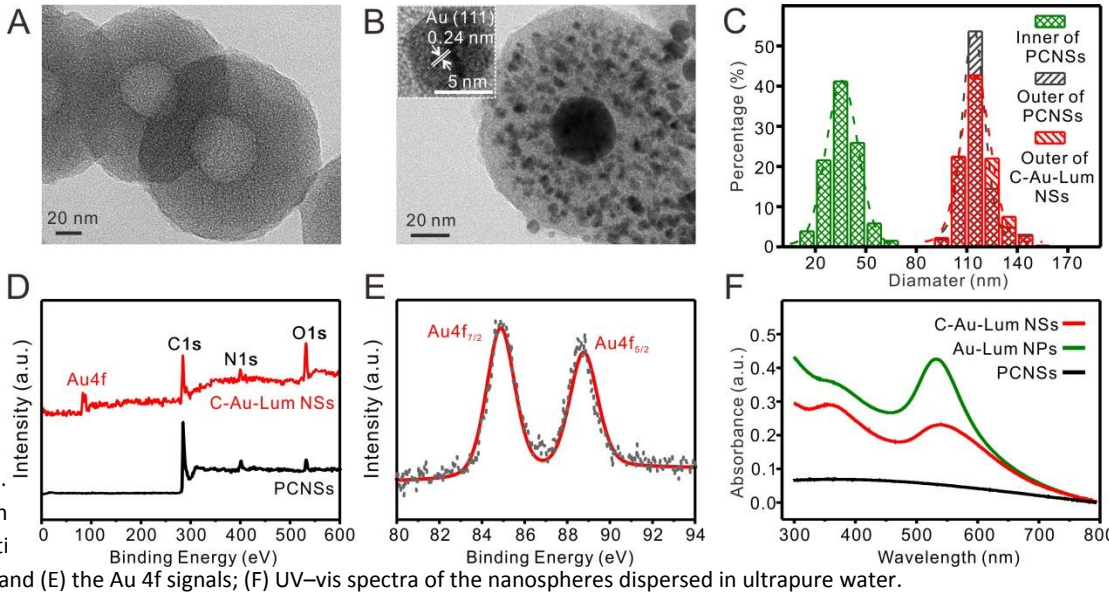

Figure 2. [illegible] t shows the represen [illegible] ge. (C) Size distributi [illegible] wide survey spectra and (E) the Au 4f signals; (F) UV–vis spectra of the nanospheres dispersed in ultrapure water.

MCH for 40 min on the electrode to block the nonspecific adsorption sites. Subsequently, 25 μL of the above st-DNA solution was coated onto the electrode for 2 h at 37 °C. Following that, the C-Au-Lum-DNA was modified on the electrode surface via the principle of complementary base pairing, which could achieve further amplification of the signal through trand displacement. The fabrication process for the proposed biosensor and corresponding signal amplification mechanism were showed in Figure 1.

ECL and EIS detection

The ECL signal of each step in biosensor construction was recorded in 0.1 M PBS (pH 8.0) containing 5 mM H_2O_2 as coreactant with a scan range from 0 to 0.8 V and a scan rate of 100 mV/s via cyclic voltammetry. The three-electrode system was consisted of an indium tin oxide electrode (ITO) as working electrode, Ag/AgCl electrode as a reference electrode and platinum wire as the auxiliary electrode. The EIS signal was measured in 0.1 M PBS (pH 7.0) containing 5.0 mM $[Fe(CN)_6]^{3-/4-}$ and 0.1 M KCl solution, the Nyquist plots was fitted by classical Randles model equivalent circuit, which consisted of the electron transfer resistance (R_{et}), the electrolyte resistance (R_s), the double layer capacitance (C_{dl}), and the Warburg impedance (Z_W). R_{et} is corresponding to the diameter of semicircular part, which could effectively control the electron transfer kinetics of $[Fe(CN)_6]^{3-/4-}$ redox probe on the electrode surface.

Results and discussion

Preparation and Characterization of PCNSs and C-Au-Lum NSs

The PCNSs obtained by direct carbonization of hollow polymer spheres exhibit hollow structure, spherical and monodispersed morphology (Figure 2A and Figure S1A) with an outer average diameter of 114.0 ± 6.4 nm (mean ± SD, n =420, Figure 2C) and a clear hollow core of 35.8 ± 9.4 nm in inner diameter. The pores inside PCNSs provide certain locations for $HAuCl_4$ reduction by luminol (Figure 1A). Luminol and its oxidative product coexisted on the surface of Au NPs through the weak covalent interaction between gold and nitrogen atoms in their amino groups[45]. The in situ formed Au-Lum NPs were restricted by nanopores of PCNSs at the same time, which successfully incorporates Lum into the nanostructure of PCNSs. The as-prepared C-Au-Lum NSs displays a solid-sphere morphology (Figure 2B and Figure S1B), and the size and mono-dispersibility (115.2 ± 8.7 nm, mean ± SD, n =478, Figure 2C) are almost identical to that of PCNSs. This indicates that the abundantly loading of Au-Lum NPs has little impact on the shape of PCNSs during the building-up procedure. Specially, HRTEM observations clearly manifest that numerous Au-Lum nanoparticles (NPs) with diameter about 7 nm are highly dispersed inside the pores and suffuse the hollow core of PCNSs (Figure 2B). The lattice spacing of Au (111) plane around 0.24 nm[47] observed in the crystalline structures of the C-Au-Lum NSs suggests that these Au-Lum NPs were stabilized in the PCNSs carriers. As a contrast, Au-Lum NPs were prepared in bulk solutions (without PCNSs) and the HRTEM and SEM images are shown in Figure S2A, B.

To further confirm the element composition, X-ray photoelectron spectroscopies (XPS) of pure PCNSs and C-Au-Lum NSs were both investigated. As shown in Figure 2D, there are three characterized peaks accountable for C 1s, N 1s and O 1s elemental species in the survey spectra of PCNSs (black curve). On the contrast, an extra peak of Au 4f expectedly appears for C-Au-Lum NSs. The Au 4f spectrum is dominated by a single peak of Au $4f_{7/2}$ at 84.8 eV and a spin-orbit doublet peak at +3.7 eV.[48] Additionally, the traces of C 1s, N 1s signals of C-Au-Lum NSs are also shown (Figure S3). The core spectrum of C 1s (Figure S3A) clearly declares four typical separated peak components, corresponding to aromatic C (284.6 eV), C-NH_2 (285.8 eV), -CO-NH- (287.4 eV) and -COO- (288.6 eV) groups, respectively.[45] The N 1s spectrum (Figure S3B) is fit with two components at 398.8 eV and 399.7 eV severally corresponding to -NH-CO- and –NH_2 groups.[45] Moreover, the TEM-EDS spectrum of C-Au-Lum NSs shows the respective atomic percentages of C, N, Au at 88.20 %, 4.40 % and 7.40 % (Figure S4). These results suggest that the Au species coupled with luminophore Lum are effectively decorated on the PCNSs to constitute C-Au-Lum NSs.

The typical UV-vis spectra were examined to confirm the formation of the as-prepared nanospheres. Observed in Figure 2F (green curve), there are two characteristic absorption peaks centered at around 360 and 530 nm for Au-Lum NPs, which are attached to luminol and Au NPs[49], respectively (Figure S5A). Notably, comparing with very weak absorption of pure PCNSs (Figure 2F, black curve), C-Au-Lum NSs exhibit these two characteristic absorption peaks (Figure 2F, red curve). This was proved by the color variation of PCNSs solution when loaded with Au-Lum NPs (Figure S5B), and further validates that PCNSs carriers are successfully decorated with Au-Lum materials.

Taken together, these combined evidences synergistically demonstrate that the decoration of PCNSs by Au-Lum NPs occurred successfully to form C-Au-Lum NSs. Plentiful Au NPs are three-dimensionally and dispersedly encapsulated in the PCNSs to immobilize luminophores Lum, therefore providing a novel idea to prepare high luminescent nanomaterials.

ECL Behaviors of C-Au-Lum NSs

C-Au-Lum NSs were modified on the ITO electrodes for ECL measurements. An obvious Gaussian-fitted ECL peak appears at 428 nm (Figure 3A, red curve) approximate to the fluorescence emission of Lum at 425 nm (the shift of 3 nm might be effected by solvents[50]). This indicates the ECL emission of C-Au-Lum NSs essentially arises from the final excited state of Lum to ground state. To acquire highly efficient light emission, the ECL spectra of C-Au-Lum NSs/ITO with different doping amount of PCNSs were displayed in Figure 3B. As expected, for a given amount of Lum, the ECL peak intensity significantly enhanced with increasingly doped PCNSs concentrations and reached a maximum when 50 ng/mL or more PCNSs were used. This demonstrates that strategy by highly dispersing luminophores on porous substrate significantly enhances the luminescent properties by increasing their availability. Therefore, the synthetic C-Au-Lum NSs with the 50 ng/mL doping amount of PCNSs was applied for follow-up experiments. The total amount of C-Au-Lum NSs of 10 µL were also quantitatively controlled, and then there were numerous C-Au-Lum NSs immobilized on the electrode for ECL measurement. In this case, the heterogeneities

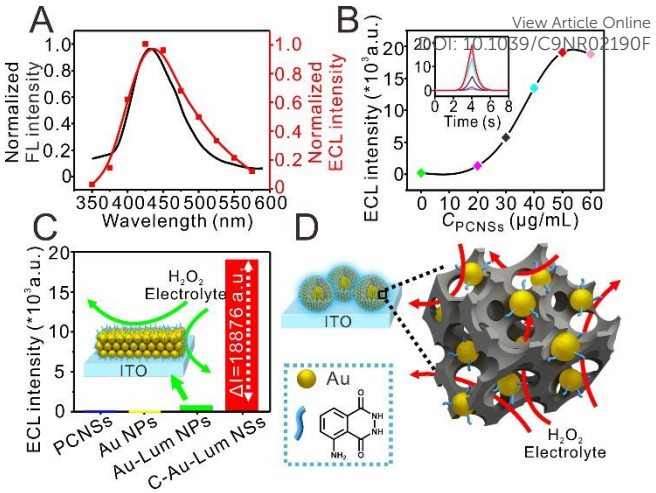

Figure 3. (A) Fluorescence spectrum of C-Au-Lum NSs (black) in ultrapure water and ECL-wavelength spectrum of C-Au-Lum NSs/ITO (red) measured through a series of optical filter (spaced 25 nm) from 350 to 575nm in 0.1 M PBS (pH 8.0) containing 5mM H_2O_2. (B) The effect of different concentration of adding PCNSs for synthesis on ECL response of C-Au-Lum NSs. Inset: ECL-time curves for different C-Au-Lum/ITO electrodes. Here the concentration of luminol was fixed at 0.16 mM and PCNSs with different amounts ranged from 0, 20, 30, 40, 50, 60 µg/mL were used. (C) ECL responses of different materials modified electrodes including PCNSs/ITO (blue), Au NPs/ITO (yellow), Au-Lum NPs/ITO (green) and C-Au-Lum NSs/ITO (red), insert is the schematic diagram of mass transfer path on Au-Lum NPs/ITO; (D) Schematic diagram of multidirectional mass transfer path

between each nanosphere could be negligible for the overall performance.

ECL performance of different nanomaterials (the fixed volume was all controlled at 10 µL) were performed and compared using 5 mM H_2O_2 as the coreactant to further quantify the enhancement capability of C-Au-Lum NSs. Almost no ECL signals were obtained from PCNSs/ITO (Figure 3C, blue column) and Au NPs/ITO (Figure 3C, yellow column) under this condition. The Au-Lum NPs/ITO manifested an anodic ECL emission at 0.79 V (Figure S6, green curve) with a weak peak intensity about 671 a.u., which is trigged by electrochemical oxidation of Lum and H_2O_2 based on well-established mechanism[51]. Remarkably, when Au-Lum NPs were decorated inside multi-pore structure of PCNSs, the C-Au-Lum NSs/ITO enabled nearly 30-fold enhancement in ECL intensity (Figure 3C, red column, 19729 a.u.) in the coincident potential (Figure S6, red curve). In view of the amounts of Lum and Au were controlled at the same level under the two circumstances, such a big difference between Au-Lum and C-Au-Lum in ECL intensity could be caused by the availability of Lum and the mass transfer of coreactant. When Au-Lum are compactly deposited on electrode surface (Figure 3C, insert), the diffusion of coreactant into the internal of the Au nano-assembly is restricted, and the ECL is mainly attributed by the outer Au-Lum. However, when the Au-Lum NPs are massively but highly dispersed into the porous structure of PCNSs with excellent conductivity (Figure 3D), the mass diffusion and electron transfer are both greatly promoted. This significantly increases the availability of the luminophores and ultimately

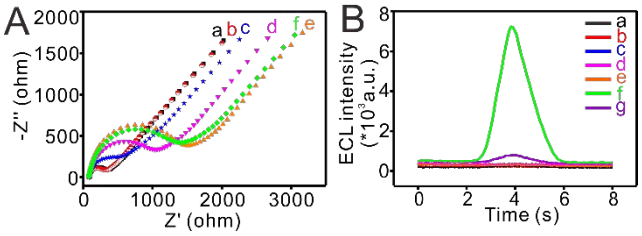

Figure 4. (A) EIS plots and (B) ECL response during the fabrication process for different modified electrodes from a-g: (a) bare ITO; (b) Au/ITO; (c) c-DNA/Au/ITO; (d) MCH/c-DNA/Au/ITO; (e) st-DNA/MCH/c-DNA/Au/ITO; (f) C-Au-Lum-DNA/st-DNA/MCH/c-DNA/Au/ITO with 100 pg/mL MUC1 target; (g) C-Au-Lum-DNA/st-DNA/MCH/c-DNA/Au/ITO without MUC1 target.

boosts the ECL signal. Besides, after continuous scanning for 8 cycles, the ECL responses of C-Au-Lum NSs remain stable with a negligible intensity fluctuation (Figure S6B) which reveals the excellent stability of the highly luminescent nanomaterials.

Construction of ECL biosensor for MUC1 detection

A dual signal amplification strategy was designed for ultrasensitive detection of the target molecule MUC1 using C-Au-Lum NSs as the ECL probe. As schematically shown in Figure 1C, MUC1 is firstly bound with its aptamer to form target-aptamer (T-A) complex. Subsequently, the T-A complex was hybridized with a-DNA to form the double strands with a blunt 3'-terminus. On this occasion, the Nt.BsmAI endonuclease cleavage action was evoked, together with the succedent T-A complex recycling process and release of numerous st-DNA fragments. The st-DNA is recognized by c-DNA immobilized on the electrode surface, and then its signal could be further amplified by proximity-initiated intermediate DNA strand displacement and detected by the ECL sensor (Figure 1B).

The construction process of ECL biosensor was investigated by electrochemical impedance spectroscopy (EIS) and the corresponding ECL signals were implemented. After electro-deposition of Au layer on the bare ITO, the electron transfer resistance (R_{et}) decreases, indicating the highly conductive Au layer coated on the electrode surface (Figure 4A, curve b). When the sulfhydryl-functionalized c-DNA was linked onto the Au/ITO surface through Au-S bond and MCH was then used to block nonspecific adsorption sites thereon, the R_{et} gradually increased (Figure 4A, curve c, d). This is owing to the electrostatic repulsion between negatively charged phosphate skeletons of DNA and $[Fe(CN)_6]^{3-/4-}$ redox probe as well as the enlarged steric hindrance. After st-DNA incubation, the hairpin structure of the c-DNA is opened by hybridization reaction, and the clogged electron transfer made the R_{et} strongly increased (Figure 4A, curve e). It is worth noting that no ECL signal was recorded in each step during all above embellishments (Figure 4B, curve a-e).

Conspicuously, with the C-Au-Lum-DNA probe assembled on the biosensor, a remarkable ECL peak appeared (Figure 4B, curve f). In this circumstance, the p-DNA on the C-Au-Lum-DNA complex was competitively hybridized with the exposed DNA fragment of c-DNA to discharge t-DNA fragments for the next circulation displacement, therefore magnifying ECL response. And the R_{et} of the biosensor slightly diminished with the incubation with C-Au-Lum-DNA probes (Figure 4A, curve f), further validating good conductivity of the ECL nanomaterials. By contrast, for the ECL bio-sensing system driven without target MUC1, only very weak ECL signal was observed (Figure 4B, curve g), which was mainly attributed to the nonspecific absorption between the signal probes and the electrode surface. These performances demonstrate that the "signal on" ECL biosensors are successfully equipped with C-Au-Lum nanomaterials for feasible MUC1 assay.

Highly Sensitive and Selective Detection of MUC1 with ECL biosensor

Here ECL response is significantly dependent on the amount of C-Au-Lum-DNA nanoprobes hybridized on the electrode during strand displacement, which is mediately controlled by the formation of st-DNA in enzymatic circulation process. Accordingly, the correlative experimental conditions were optimized. As depicted in Figure S7, the Nt.BsmAI endonuclease of 54 U/mL at cleavage time of 120 min coupled with p-DNA of 0.4 μM at incubation time of 80 min were finally determined to achieve the best ECL performance for MUC1 detection. Under the optimal conditions, the sensitivity of the ECL biosensor was studied in target MUC1 standard samples with a series of concentrations. Figure 5A illustrates that with an increasing concentration of MUC1, the ECL peak intensity enhanced simultaneously. This is mainly due to the fact that the more MUC1 there was, the more st-DNA fragments were released after enzymatic circulation, which could open more

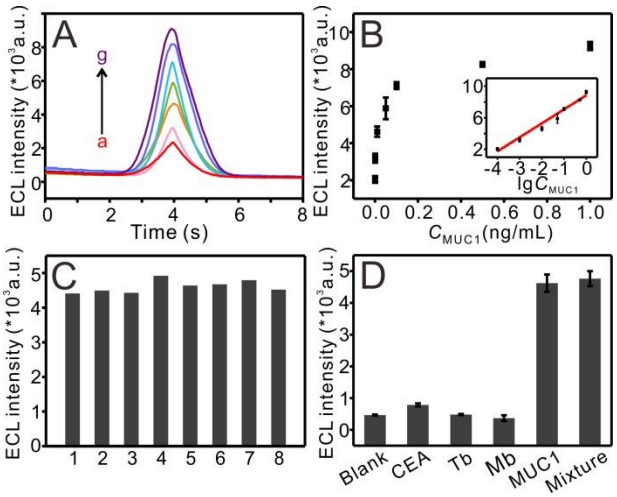

Figure 5. (A) ECL response of the proposed biosensor in the presence of different concentrations of MUC1 from a to g: 0.1, 1, 10, 50, 100, 500 and 1000 pg/mL; (B) The relationship between ECL intensity and the concentration of MUC1, inset: the calibration plots of ECL signal versus the logarithm of the MUC1 concentration; (C) Reproducibility of the proposed ECL biosensor with eight ITO for the detection of 10 pg/mL MUC1; (D) ECL responses for three potential interferences in human serum: the blank, CEA (100 pg/mL), Tb (100 pg/mL), Mb (100 pg/mL), and mixture containing three aforementioned interferences and MUC1 of 10 pg/mL. All the ECL signals were recorded in PBS (0.1 M, pH 8.0) containing 5 mM H_2O_2. The PTM was set at 800 V and the potential scan was from 0 to 0.8 V at scan rate of 100 mV/s.

harpin-structure c-DNA, leading to large amount of C-Au-Lum-DNA hybridized onto the sensor's surface. The ECL intensity is linearly depended on the logarithm values of different MUC1 concentrations ranged from 0.1 pg/mL to 1 ng/mL with a correlation coefficient of 0.994 (Figure 5B). The detection limit was calculated to be 47.6 fg/mL (S/N = 3) with the regression equation as I_{ECL}=1773.33lg$c$+8835.46. Comparing with previous reported assays, the superior detection sensitivity of the proposed ECL biosensor was achieved (Table S2), certifying the admirable ECL property of C-Au-Lum NSs probe and effective dual signal amplification strategies. Furthermore, a RSD value of 3.6 % was gained with eight parallel measurements in 10 pg/mL MUC1 (Figure 5C), showing the favorable reproducibility of this assay.

To evaluate the selectivity of ECL biosensor in complex biological matrices, several proteins existed in human serum including CEA, Tb, and Mb at the concentration of 100 pg/mL were added as potential interferences into the sensing system. The respective ECL response in Figure 5D was negligible comparing with control experimental result of blank sample. Notably, the specific target MUC1 existed even at the 10-fold lower concentration of 10 pg/mL alone or mixed with interferences could cause drastically ECL enhancement. These performances demonstrated that ECL signal of the proposed biosensor was specifically generated from the faithful hybridization of aptamer and MUC1 target, manifesting high selectivity for the target protein discrimination.

Real Serum Samples Determination

The applicability of the proposed ECL biosensor in real human serum samples was assessed by standard addition method. With standard MUC1 solution with different concentrations (0.1, 1, and 10 pg/mL) were severally injected into 10-fold diluted human serum, the recoveries were calculated to be 96.4 %, 104.0 %, and 95.0 % with the responding RSD from 1.8 % to 7.5 % (Table 1), suggesting the feasibility of the ECL biosensor for monitoring targets in complicated biological samples.

Table 1. Determination of MUC1 in 10-diluted human serum by the proposed ECL biosensor (n=3).

Sample name		Added (pg/mL)	Found (pg/mL)	Recovery (%)	RSD (%)
serum	1	0.1	0.0964	96.4	7.5
	2	1	1.04	104.0	3.6
	3	10	9.50	95.0	1.8

Conclusion

In summary, we developed a novel strategy to enhance ECL emission by highly dispersing luminophores into porous and highly conductive carbon nanomaterials. By this means, the mass transfer of regents and electron transport can be significantly accelerated inside porous nanospheres, therefore greatly improving the utilization ratio of luminophores and enhancing the ECL signal. Further integration with dual signal amplification strategy of enzymatic circulation and strand displacement, a ultrasensitive and highly selective ECL platform for MUC1 monitoring could be readily accomplished with a detection limit as low as 47.6 fg/mL. Meanwhile, the feasibility was verified by satisfactory recoveries of targets MUC1 in human serum samples. In view of the excellent ECL performance of the as-prepared luminescent nanospheres and the versatility of the aptamer-based recognition, this study provides new ideas in high-efficient ECL sensing system design for bioassay and clinical diagnoses.

Conflicts of interest

The authors declare no competing financial interest.

Acknowledgements

This work was supported by the National Natural Science Foundation of China (Nos. 31501568, 11674085, 21725504).

References

1 M. A. Hollingsworth and B. J. Swanson, *Nat. Rev. Cancer*, 2004, **4**, 45-60.
2 D. W. Kufe, *Nat. Rev. Cancer*, 2009, **9**, 874-885.
3 V. J. Somovilla, I. A. Bermejo, I. S. Albuquerque, N. Martínez-Sáez, J. Castro-López, F. García-Martín, I. Compañón, H. Hinou, S. Nishimura, J. Jiménez-Barbero, J. L. Asensio, A. Avenoza, J. H. Busto, R. Hurtado-Guerrero, J. M. Peregrina, G. J. L. Bernardes and F. Corzana, *J. Am. Chem. Soc.*, 2017, **139**, 18255-18261.
4 M. S. Nabavinia, A. Gholoobi, F. Charbgoo, M. Nabavinia, M. Ramezani and K. Abnous, *Med. Res. Rev.*, 2017, **37**, 1518-1539.
5 J. Feng, X. Wu, W. Ma, H. Kuang, L. Xu and C. Xu, *Chem. Commun.*, 2015, **51**, 14761-14763.
6 C. S. M. Ferreira, K. Papamichael, G. Guilbault, T. Schwarzacher, J. Gariepy and S. Missailidis, *Anal. Bioanal. Chem.*, 2008, **390**, 1039-1050.
7 Y. He, Y. Lin, H. Tang and D. Pang, *Nanoscale*, 2012, **4**, 2054.
8 X.-P. Liu, P.-P. Li, C.-J. Mao, H.-L. Niu, J.-M. Song and B.-K. Jin, *Sens Actuators B Chem.*, 2018, **275**, 251-259.
9 S. Yang, F. Zhang, Q. Liang and Z. Wang, *Biosens. Bioelectron.*, 2018, **120**, 85-92.
10 W. Wei, D. F. Li, X. H. Pan and S. Q. Liu, *Analyst*, 2012, **137**, 2101-2106.
11 G.-B. Hu, C.-Y. Xiong, W.-B. Liang, X.-S. Zeng, H.-L. Xu, Y. Yang, L.-Y. Yao, R. Yuan and D.-R. Xiao, *ACS Appl. Mater. Interfaces*, 2018, **10**, 15913-15919.
12 N. E. Tokel, A. J. Bard, *J. Am. Chem. Soc.*, 1972, **94**, 2862-2863.
13 A. J. Bard, Electrogenerated Chemiluminescence; Marcel Dekker: New York, 2004.
14 W. Miao, *Chem. Rev.*, 2008, **108**, 2506-2553.
15 Z. Liu, W. Qi and G. Xu, *Chem. Soc. Rev.*, 2015, **44**, 3117-3142.
16 W. Wen, X. Yan, C. Zhu, D. Du and Y. Lin, *Anal. Chem.*, 2017, **89**, 138-156.
17 M.-M. Chen, Y. Wang, S.-B. Cheng, W. Wen, X. Zhang, S. Wang and W.-H. Huang, *Anal. Chem.*, 2018, **90**, 5075-5081.
18 Z. Wu, J. Hu, T. Zeng, Z.-L. Zhang, J. Chen, G. Wong, X. Qiu, W. Liu, G. F. Gao, Y. Bi and D.-W. Pang, *Anal. Chem.*, 2017, **89**, 2039-2048.
19 S. Carrara, F. Arcudi, M. Prato and L. De Cola, *Angew. Chem. Int. Ed.*, 2017, **56**, 4757-4761.
20 J. Wang, Z. Peng, J. Yang, X. Wang and N. Yang, *Talanta*, 2008, **75**, 817-823.

View Article Online
DOI: 10.1039/C9NR02190F

21 Y. Dong, H. Wu, P. Shang, X. Zeng and Y. Chi, *Nanoscale*, 2015, **7**, 16366-16371.
22 L. Li, M. Li, Y. Sun, J. Li, L. Sun, G. Zou, X. Zhang and W. Jin, *Chem. Commun.*, 2011, **47**, 8292-8294.
23 J.-L. Liu, M. Zhao, Y. Zhuo, Y.-Q. Chai and R. Yuan, *Chem. Eur. J.*, 2017, **23**, 1853-1859.
24 G.-Y. Zhang, C. Cai, S. Cosnier, H.-B. Zeng, X.-J. Zhang and D. Shan, *Nanoscale*, 2016, **8**, 11649-11657.
25 C.-Y. Xiong, H.-J. Wang, W.-B. Liang, Y.-L. Yuan, R. Yuan and Y.-Q. Chai, *Chem. Eur. J.*, 2015, **21**, 9825-9832.
26 H.- Zhou, J. R. Long and O. M. Yaghi, *Chem. Rev.*, 2011, **112**, 673-674.
27 K. Wang, D. Feng, T.-F. Liu, J. Su, S. Yuan, Y.-P. Chen, M. Bosch, X. Zou and H.-C. Zhou, *J. Am. Chem. Soc.*, 2014, **136**, 13983-13986.
28 S. Ge, L. Zhang, Y. Zhang, F. Lan, M. Yan and J. Yu, *Nanoscale*, 2017, **9**, 4366-4382.
29 F. Xu, Z. Tang, S. Huang, L. Chen, Y. Liang, W. Mai, H. Zhong, R. Fu and D. Wu, *Nat. Commun.*, 2015, **6**, 7221.
30 J. Du, L. Liu, Z. Hu, Y. Yu, Y. Qin and A. Chen, *Adv. Funct. Mater.*, 2018, **28**, 1802332.
31 F. Schüth and W. Schmidt, *Adv. Mater.*, 2002, **9**, 629-638.
32 A. Ragusa, I. Garcia and S. Penades, *IEEE T Nanobiosci*, 2007, **6**, 319-330.
33 Z. Hu, B. J. Deibert and J. Li, *Chem. Soc. Rev.*, 2014, **43**, 5815-5840.
34 H. Zhao, G. Yu, M. Yuan, J. Yang, D. Xu and Z. Dong, *Nanoscale*, 2018, **10**, 21466-21474.
35 P. Shang, J. Zhang, W. Tang, Q. Xu and S. Guo, *Adv. Funct. Mater.*, 2016, **26**, 7766-7774.
36 R. J. White, R. Luque, V. L. Budarin, J. H. Clark and D. J. Macquarrie, *Chem. Soc. Rev.*, 2009, **38**, 481-494.
37 A. Primo and F. Quignard, *Chem. Commun.,* 2010, **46**, 5593-5595.
38 Y. Zhou, J. Wang, Y. Hu, R. O'Hayre and Z. Shao, *Chem. Commun.,* 2010, **46**, 7151.
39 L. Chen, J. Yan, Z. Tong, S. Yu, J. Tang, B. Ou, L. Yue and L. Tian, *Micropor. Mesopor. Mat.*, 2018, **266**, 126-131.
40 W. Qi, D. Wu, J. Zhao, Z. Liu, W. Zhang, L. Zhang and G. Xu, *Anal. Chem.*, 2013, **85**, 3207-3212.
41 X. Dong, G. Zhao, L. Liu, X. Li, Q. Wei, W. Cao, *Biosens. Bioelectron.*, 2018, **110**, 201-206.
42 Y. Zhang, S. Deng, J. Lei, Q. Xu, H. Ju, *Talanta*, 2011, **85**, 2154-2158.
43 A.-H. Lu, T. Sun, W.-C. Li, Q. Sun, F. Han, D.-H. Liu and Y. Guo, *Angew. Chem. Int. Ed.*, 2011, **50**, 11765-11768.
44 R. J. White, K. Tauer, M. Antonietti and M. Titirici, *J. Am. Chem. Soc.*, 2010, **132**, 17360-17363.
45 H. Cui, W. Wang, C.-F. Duan, Y.-P. Dong and J.-Z. Guo, *Chem. Eur. J.,* 2007, **13**, 6975-6984.
46 Z. Xu, L. Liao, Y. Chai, H. Wang and R. Yuan, *Anal. Chem.*, 2017, **89**, 8282-8287
47 W. Luo, C. Zhu, S. Su, D. Li, Y. He, Q. Huang and C. Fan, *ACS Nano*, 2010, **4**, 7451-7458.
48 M. F. Lengke, M. E. Fleet and G. Southam, *Langmuir*, 2006, **22**, 2780-2787.
49 Y. Cheng, Y. Huang, J. Lei, L. Zhang and H. Ju, *Anal. Chem.*, 2014, **86**, 5158-5163.
50 Y. Feng, F. Sun, N. Wang, J. Lei and H. Ju, *Anal. Chem.*, 2017, **89**, 7659-7666.
51 S. Sakura, *Anal. Chim. Acta*, 1992, **262**, 49-57.

Table of Contents Entry

View Article Online
DOI: 10.1039/C9NR02190F

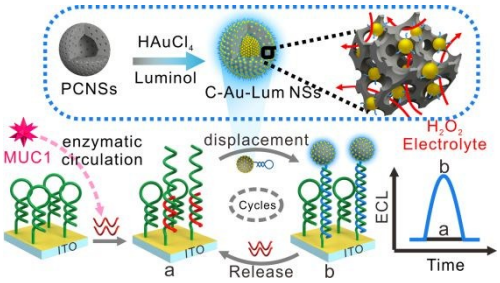

We propose a novel strategy by high dispersion of luminophores inside porous carbon nanospheres for ultrasensitive electrochemiluminescent detection of MUC1